INTERNATIONAL ATOMIC ENERGY AGENCY
UNITED NATIONS EDUCATIONAL, SCIENTIFIC AND CULTURAL ORGANIZATION
INTERNATIONAL CENTRE FOR THEORETICAL PHYSICS
I.C.T.P., P.O. BOX 586, 34100 TRIESTE, ITALY, CABLE: CENTRATOM TRIESTE

H4.SMR/453-4

TRAINING COLLEGE ON PHYSICS AND CHARACTERIZATION OF LASERS AND OPTICAL FIBRES

(5 February - 2 March 1990)

Airborne Lidar Detection of Subsurface Oceanic Scattering Layers

F. Hoge

NASA Goddard Space Flight Center
Wallops Flight Facility
Wallops Island, Virginia
U.S.A.

Airborne lidar detection of subsurface oceanic scattering layers

Frank E. Hoge, C. Wayne Wright, William B. Krabill, Rodney R. Buntzen, Gary D. Gilbert, Robert N. Swift, James K. Yungel, and Richard E. Berry

The airborne lidar detection and cross-sectional mapping of submerged oceanic scattering layers are reported. The field experiment was conducted in the Atlantic Ocean southeast of Assateague Island, VA. NASA's Airborne Oceanographic Lidar was operated in the bathymetric mode to acquire on-wavelength 532-nm depth-resolved backscatter signals from shelf/slope waters. Unwanted laser pulse reflection from the air–water interface was minimized by spatial filtering and off-nadir operation. The presence of thermal stratification over the shelf was verified by the deployment of airborne expendable bathythermographs. Optical beam transmission measurements acquired from a surface truthing vessel indicated the presence of a layer of turbid water near the sea floor over the inner portion of the shelf.

I. Introduction

The terrestrial biomes, oceans, and troposphere form the major global pools of carbon, nitrogen, sulfur, and phosphorus. The present state of these elemental pools and the fluxes between them must be accurately determined if we are to effectively establish man's influence on the future state of the major biogeochemical cycles. One of the best methods to study global phenomena is from spaceborne platforms. Accordingly, the U.S. National Academy of Sciences has thus established that the highest priority objective for the study of the global biogeochemical cycles from space is to accomplish several important goals, one of which is the measurement of the concentration of chlorophyll *a* in the world's oceans.[1] Our lidar program (of which the work described herein is a part) addresses the measurement of oceanic constituents and water optical properties in general and the active–passive measurement of phytoplankton pigments specifically.

Recent models show progress in relating satellite-derived chlorophyll to oceanic primary production.[2] Since the oceans account for about one-third of the total global plant fixation of carbon,[3] accurate remote measurements are required to both establish and improve total productivity estimates. As suggested by the ocean science community, the satellite data should be validated by a modest sea truth activity.[4]

The most serious reservations about remotely sensed chlorophyll data have been recently summarized.[4] First, such satellite sensors view or detect only a small fraction of the total phytoplankton biomass in the upper water column (5% or less, accounting for up to 11% of the biomass turnover). Second, satellite data miss the peaks of the vertical distribution of biomass and production.[5] Third, all information of the vertical structure is lost. In spite of these limitations, it is generally felt that there is a role for satellite-derived chlorophyll measurements and primary production estimates in regional oceanographic applications, provided that a supporting sea-truthing program is carried out as well.[4]

Research vessels have generally been employed to provide the surface truthing measurements essential to the quantitative interpretation of satellite ocean color imagery. A well-equipped research vessel is capable of making very accurate measurements of a large number of physical, chemical, and biological parameters. Moreover these measurements can be extended into the water column to provide the vertical distribution of these parameters. Unfortunately, research vessels have a significant limitation: their speed severely restricts the area of coverage. Accordingly, as the ship steams within a satellite-imaged area, the

Richard Berry is with Indiana University of Pennsylvania, Indiana, Pennsylvania 15705; R. N. Swift and J. K. Yungel are with EG&G Washington Analytical Services, Inc., Pocomoke, Maryland 21851; R. R. Buntzen and G. D. Gilbert are with Naval Ocean Systems Center, San Diego, California 92152; and the other authors are with NASA Goddard Space Flight Center, Wallops Flight Facility, Wallops Island, Virginia 23337.

Received 25 March 1988.

simultaneity of the satellite-ship data continually diminishes. To partially overcome this problem, more ships can be used. However, the cost of using more and more vessels eventually dilutes the attractiveness of the very satellite method itself.

More recently, instrumented aircraft have been utilized in coordinated experiments involving ship and satellite platforms. The aircraft is used in conjunction with the research vessel(s) to significantly extend their area of contemporaneous truthing within the satellite image. The measurements made from the research vessel are used to ensure the validity of the low flying airborne sensor measurement. The speed of the aircraft (15–25 times that of the research vessel) allows the extension of the validated measurement over wide areas. Present capabilities of aircraft sensors for supporting satellite ocean color applications are, however, restricted to the upper surface layer. Active laser-induced fluorosensor chlorophyll measurements are essentially restricted to the upper several meters of the water column,[6] while passive ocean color observations include the integration of information coming from deeper in the surface layer.[7] To utilize the full potential afforded by the speed of an aircraft platform, instrumentation and techniques need to be developed to extend the phytoplankton photopigment measurement capability of the airborne sensors into the water column.

The objective of the work described herein was to initiate the development of airborne lidar techniques for depth resolving chlorophyll concentration and the distribution of scattering layers in marine waterbodies. Previous investigations in the U.S.A.,[8] Canada,[9] Sweden,[10] and Australia[11] have established that accurate hydrographic determinations to depths in excess of 30 m can be achieved with properly equipped airborne lidar systems in clear/low turbidity conditions.[12] In these applications, the on-wavelength backscatter from a blue-green laser transmitter is temporally resolved between the ocean surface and bottom. The scattering layer investigations involve refinement of these airborne hydrographic techniques to allow an assessment of the vertical distribution of particulate matter within the water column. With further improvements in instrumentation and techniques and the addition of a second laser wavelength, the acquisition of depth resolved reflectances at two wavelengths could be retrieved. Then, two-band algorithms, similar to those now in use with passive upwelled spectral radiances, could be used to determine the vertical structure of chlorophyll. The scattering layer investigations were also executed to examine the feasibility of detecting and measuring internal waves from modulation in the pattern of lidar backscatter returned from particulate layers. In certain water masses, development of a persistent scattering layer at the maximum density gradient near the top of the thermocline is expected to provide sufficient backscatter cross section to be resolved by a properly equipped airborne lidar system.

The airborne lidar observations described in this paper were confined to night flights to improve the SNR and thus establish the feasibility of the lidar methodology. With additional development, depth-resolved lidar backscatter data could be obtained in daylight conditions together with spectral radiances. Variations of correlation spectroscopy methods such as those recently developed by Hoge and Swift[13] could then be utilized to relate the ocean color observations to the scattering layer and vertical chlorophyll measurements to provide a more solid understanding of the integrated ocean color signals.

Observations of particulate matter extending to the bottom of the mixed layer have been made using acoustic echo-sounding instrumentation[14] from a moving ship. Also, particulate matter and/or acoustic index of refraction variations have been observed from ship track data and corroborated by aircraft and satellite observations.[15,16] Shipboard lidar remote sensing of internal waves and optical properties has only been reported recently.[17]

Airborne on-wavelength depth-resolved laser return signals have been used to provide a measurement of the effective attenuation of the water column.[18] During the coarse of airborne laser bathymetry and water-optical-properties measurement experiments two layers of water with markedly different turbidity characteristics were apparently detected in one vertical column of water.[11] However, no cross-sectional display or presentation of the phenomena was given. The airborne detection of oceanic turbidity cell structure has also been reported through the use of depth-resolved laser-induced water Raman backscatter.[19]

We report here, for the first time, the airborne lidar detection and cross-sectional mapping of a subsurface oceanic plume. This feature extended for several kilometers in an on-shore/off-shore direction. The field investigation was conducted during early June 1986 as a cooperative endeavor between the National Aeronautics and Space Administration and the Naval Ocean Systems Center. The flights were part of a longer range program designed to develop the capability of detecting and measuring the spatial distribution of scattering layers in open ocean environments. This initial flight was aimed at evaluating various electrooptical components in the AOL system and their compatibility with a high-powered Nd:YAG laser. The flight was a precursor to making a number of modifications necessary to optimize the sensor to meet the scattering layer measurement program objectives. In conducting this initial experiment, some changes to the existing electrooptical system were necessary. These changes are described in the next section. We realize that the system, as configured for the investigations described herein, was less than ideal for making scattering layer measurements and that improvements to the sensor over the next several years will significantly improve the results. Nonetheless, the results thus far serve as a notable milestone and are sufficiently encouraging to warrant the continued development of the sensor for the scattering layer application.

II. Airborne Lidar Instrumentation Description

The NASA Airborne Oceanographic Lidar (AOL) was used to obtain the field data presented here. The AOL and associated equipment were flown on a four-engine NASA P-3A aircraft from Goddard Space Flight Center (GSFC) Wallops Flight Facility. The AOL has been discussed in detail in papers dealing with various marine applications including other chlorophyll mapping field experiments[20–23] as well as oil spill,[24,25] tracer dye,[26] oceanic turbidity cell structure,[19] water depth,[8] and laser backscatter[27,28] measurement investigations. The AOL is also capable of performing terrestrial investigations[29,30] including leaf fluorescence.[31] The AOL also contains a passive ocean color subsystem (POCS),[32] which is applicable to the measurement of oceanic pigments.[33] The POCS instrumentation was not used in these experiments, but this or a similar spectroradiometer could be used for the correlative studies of depth-resolved backscatter and passive ocean color as discussed in Sec. I.

Several new modifications to the AOL were made to execute the scattering layer experiments described herein. Since the changes have not been previously reported in any of the above referenced AOL papers, a brief narrative is provided here. A Spectra-Physics DCR-2 laser was used as a transmitter source in this experiment. The frequency-doubled output (532 nm) of the laser provided a 5-ns pulse (measured at half of the maximum pulse amplitude) at 300 mJ energy/pulse. Although the laser is capable of operation at 20 pulses per second (pps), it was operated at 10 pps during the scattering layer experiments because the existing cooling equipment onboard the P-3A did not have sufficient capacity to support sustained operation at 20 pps. A 10-cm (4-in.) square 5-nm bandwidth interference filter (centered at 532 nm) was inserted in front of the photomultiplier to reject any small amount of ambient light encountered during the night mission.

Figure 1 gives the new orientation of the AOL optical table in the NASA P-3A aircraft. It is shown horizontally rotated 90° from its previous position[32,33] to bring the laser beam directly out of the aircraft using only a single folding mirror. The AOL scan mirror and companion scan-folding mirror were not needed in this investigation. The two-mirror scanning assembly was removed to eliminate signal losses introduced by the additional mirrors and to avoid damage to the mirror surfaces from the high-powered frequency-doubled Nd:YAG laser. The elimination of the scanning system also helped avoid adverse effects to the receiver components produced as a result of strong laser backscatter from these additional mirror surfaces. The removal of the scan mirror assembly also necessitated that the entire optical table be canted ~5° (forward) relative to the floor of the aircraft to utilize an existing port in the aircraft. The 5° tilt combined with the ~2° nose-up attitude of the aircraft during flight results in a ~7° off-nadir incidence angle with respect to the mean ocean surface. This off-nadir incidence angle of the transmitted laser beam significantly reduces the strong Fresnel reflection originating at the air–water interface. The increased dynamic range of the total backscattered signal introduced by this strong surface reflection is a major impediment to the straightforward detection of scattering layers.

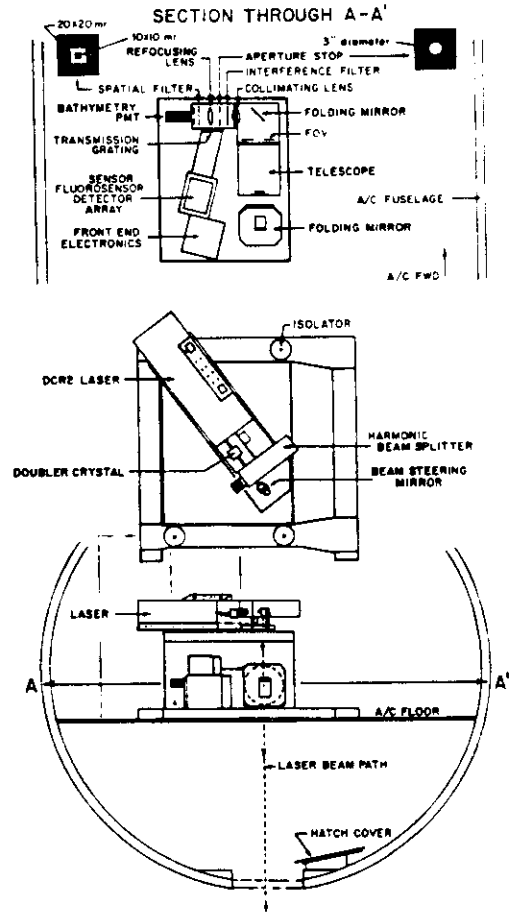

Fig. 1. Optical and mechanical configuration of the AOL in the P-3A aircraft during the conduct of the scattering layer experiments. The aperture stop and spatial filter were added to the usual optical train to improve the rejection of the strong Fresnel reflection at the air–water interface. The laser is positioned diagonally on the optical table for added mechanical strength and to allow the beam to exit the aircraft after only a single mirror reflection.

To further reduce the strong surface reflection prior to its detection by the photomultiplier tube, a spatial filter was placed in the optical train. The desired position for the spatial filter was at the telescope focal plane. However, the arrangement of receiver optical components in the AOL system at the time of these preliminary scattering layer experiments precluded installation of the spatial filter at the telescope focal plane without significant modifications of the optical components. Accordingly, a less optimal position was temporarily selected at a secondary focal plane just ahead of the repositioned bathymetry photomultiplier tube. Its location is also shown in Fig. 1. The spatial filter was an opaque obscuration matched to the diameter of the brightest portion of a laser illuminated 150-m distant target surface (as viewed by the optical sys-

tem). The planar outline of the spatial filter was originally ink-drawn on a transparent optical substrate while directly viewing the laser-irradiated target board. Several square-area spatial filters (Fig. 1) having varying spot sizes were constructed to allow some limited degree of experimentation during the flight. More sophisticated photographic methods applied in the telescopic focal plane would no doubt allow a more optimal filter to be developed. Ground test results indicated that the image in the secondary focal plane was not adequately focused to permit a reasonably complete obscuration of the laser footprint. The insertion of an aperture stop (Fig. 1) in front of the lens that forms the secondary image was found to increase the effectiveness of the spatial filter and was, therefore, included in the instrument configuration.

The inclusion of the spatial filter and field stop was a relatively crude measure performed to allow the acquisition of requisite engineering data from which an evaluation of the increased dynamic range afforded by such measures could be assessed. Follow-on tests to design and engineer the spatial filter into the telescope focal plane are currently being conducted. Placement of the spatial filter in the telescope focal plane is expected to provide much improved results. The aperture stop reduces signal levels and is not expected to be necessary when the spatial filter is located at the telescope focal plane.

The unusual diagonal orientation of the laser head on the AOL optical table was used to provide more mechanical support without utilizing additional heavy support brackets. The AOL beam-split mirror and fluorosensor spectrometer were not used in these initial experiments since only the bathymetry mode of the instrument was being used.

The usual AOL bathymetry waveform acquisition electronics[8] were utilized only for data validation. The 5-ns aperture of the thirty-six LeCroy 2249-SG digitizers and the 180-ns data collection window were both considered insufficient for performing scattering layer measurements. Instead a Tektronix R-7912 high-resolution waveform digitizer was used to depth resolve the on-wavelength backscatter data. The R-7912 digitizer was set to sample the return waveform at 1-ns intervals over a 512-ns window. The digitization of the signal was set to begin some 50-ns prior to the arrival of the surface return so that the entire surface return could be captured in the waveform information. The R-7912 digitizer was separately interfaced to a Heurikon model HK68/ME and HK68/M10 multibus minicomputer. To compensate for the exponential decay of the signal within the upper portion of the water column, the gain of the R-7912 digitizer was set to digitally saturate the signal from surface return and the upper portion of the water column. The analog signal was kept below the saturation limit of the PMT.

The temporal measurements from the R-7912 digitizer were routed to a Heurikon multibus computer and were recorded on a computer compatible tape along with time of day to millisecond resolution. The time of day was received from the same digital clock

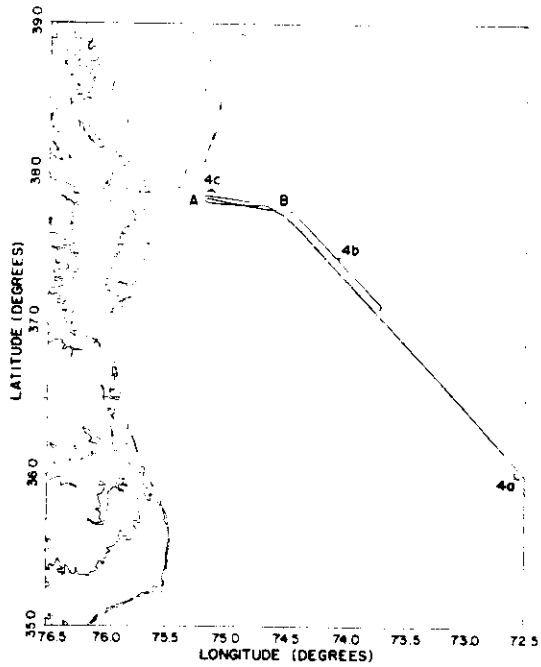

Fig. 2. Location of the various experiment flight lines executed during the scattering layer experiment. The segments labeled 4*a*, 4*b*, and 4*c* are geographical locations of the scattering layer profile panels illustrated in grey tone in Fig. 4 and in color on the front cover.

utilized by a Hewlett Packard (HP) 1000-E series minicomputer, which was used to record the remaining digital information, including slant range, Loran-C positions, aircraft attitude, and position from an inertial navigation system (INS), and the output from an airborne expendable bathythermograph (AXBT) subsystem. The AXBTs were launched at various intervals along the flight line to provide the vertical temperature structure as a function of depth.

III. Airborne Field Experiment Description

The results given herein were obtained during an airborne field experiment conducted in an area of the Atlantic Ocean southeast of Wallops Island, VA. The location of the flight experiment is shown in Fig. 2. The observations were acquired over a number of differing water mass including near-coastal, shelf, slope, and Sargasso Sea waters. The mission was performed on the night of 10 June 1986. The flight commenced ~1 h after sunset. However, the pass from which the results were presented in this paper was flown ~2.5 h after sunset.

The flight tracks indicated in Fig. 2 were designed to originate near the shoreline, to cross a relatively shallow stretch of shoals which parallel the coast, and to extend seaward into areas where comparatively clear water (outer shelf, slope, and Sargasso Sea) was known to exist. The shoals were included in the flight track so that at least some portion of the sea floor would be measured in the temporal waveform captured by the lidar system. This would provide an independent record of the instrument performance that could be related to previous experience in bathymetry experi-

ments, which in turn could be used to gauge the relative strength of any scattering layer signals acquired in the near shore area.

Surface truthing measurements were obtained at five stations along the inner portion of the flight line. The surface truthing observations were made from a locally chartered vessel outfitted with a hydraulic winch and cargo boom. Optical measurements were obtained at a number of depths between the surface and bottom with a beam transmissometer. Diffuse attenuation coefficient measurements were made with an irradiance meter at three of the stations occupied during daylight conditions. The optical measurements acquired with the beam transmissometer will be subsequently discussed along with the airborne results. The data from the irradiance meter would require processing before further analysis is undertaken.

Unfortunately, due to several logistical problems over which we had no control, many of the ship and aircraft observations were not coincident in either time or space. Thus a large portion of the truthing data obtained during the airborne field experiment was not concurrent enough to utilize for directly verifying the airborne lidar measurements. However, the truthing measurements can be utilized for verifying the presence of submerged scatterers within the study area.

IV. Description of Results

The first three passes of the mission were largely consumed in optimizing the lidar system for making the scattering layer measurements and thus were not processed. During these passes, several different size spatial filters were inserted into the secondary focal plane to determine the most effective size for damping the surface return while retaining a reasonably high SNR for measuring the volume backscatter. Since computerized methods for quality control had not been developed for this application, the selection of the most effective spatial filter size was empirically derived from viewing a digital scope trace of the R-7912 temporal waveform. The flight line, shown in Fig. 2, began at point A (~2 km off the beach) and extended into the Sargasso Sea with a dogleg at B. Passes 1 and 3 were flown from west to east, while passes 2 and 4 were flown in the reverse direction. Passes 1 and 2 were shortened to provide coverage only between points A and B. Only the results from pass 4 are discussed in this paper and labeled within Fig. 2.

A distinct region of elevated laser return from a scattering layer in the vicinity of the shoals flanking Assateague Island was noted on all passes. The strong signal from the scattering layer was easily discerned since a separate return from the ocean floor was also apparent in the digital waveform. A typical waveform from the inner portion of the flight line is shown in Fig. 3. The locations of the reflected signal from the ocean bottom and return signal from the scattering layer are labeled within the figure. As expected, the width of the bottom return is considerably narrower than the return pulse from the scattering layer. Notice that the surface return from the air–water interface is off-scale.

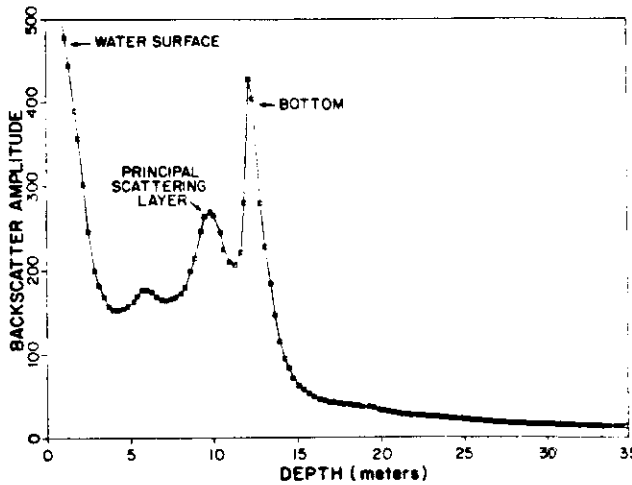

Fig. 3. Typical on-wavelength backscatter waveform obtained during transect over the shoal region identified as segment 4c in Fig. 2. The location of the waveform is also labeled W in the density profile shown in Fig. 4(c).

As previously discussed, to ensure the resolution of volumetric features it was necessary to increase the gain of the R-7912 to the point where the surface return signal was digitally saturated (higher than the 10-bit maximum resolution of the R-7912) by 5–10×.

A persistent increase in backscatter from layers within the ocean volume was observed over the entire inner shelf from B (Fig. 2) landward. Patchy returns were also detected at various points along the outer shelf and slope water masses, especially in the slope water adjacent to the Gulf Stream. The strength of backscatter from layers in the outer shelf and slope were considerably weaker and more difficult to quantify because of the rather significant system response to the large surface return and near surface signals. Ideally, deconvolution techniques[19] which separate the system response function from the actual total temporal backscattered lidar signal recorded by the AOL should be used to process the individual waveforms. However, the amplification of the surface return portion of the backscattered waveform into digital saturation prevented the application of this formal approach. Instead, a simple environmental subtraction technique was used to demonstrate the adequacy of some of the lidar system components for the scattering layer investigation and to prove the general feasibility of the airborne methodology. The environmental subtraction technique was originally developed and found to be successful for processing bathymetric data.[8]

Briefly, this technique involves developing a computer matrix look-up table based on observations made in regions known to have extremely low levels of particulate scattering and to subsequently subtract these waveforms from those waveforms obtained in areas where heavier particulate loading is expected to be present. In practice, the amplitude of the surface return is known to produce system related temporal

artifacts in the bathymetric waveform which are reproducible. In previous applications of this technique, a key channel located near the peak of the surface return was used to match clear water waveforms with similar amplitude waveforms containing particulate backscatter. However, due to the necessity to digitally saturate the surface return, it was necessary to instead select a channel on the trailing edge of the surface return to serve this purpose.

Prior to processing and plotting, the 512-channel digital waveforms were resampled with a simple five-channel block average. This resulted in 102 channels each 5 ns wide. The averaging was done to reduce channel-to-channel noise and to decrease the computer memory requirements for the clear water matrix utilized in the environmental subtraction process. The clear water matrix is developed by averaging waveforms obtained in the Sargasso Sea into groups determined according to the amplitude of the key channel. The matrix contains some fifty equally spaced groups arranged between twenty and 1000 counts. During data processing the appropriate clear water waveform (based on the amplitude of the key channel in the waveform under consideration) is developed through interpolation from the matrix look-up table. This interpolated waveform is subsequently subtracted from the individual waveform to produce a residual waveform. Since both the observed and interpolated waveforms possess the system response function almost equally, the residual waveform can be considered approximately a measure of the actual difference in volume backscatter. Accordingly, variations seen in along-track plots of the backscatter density developed from the residual waveforms indicate differences in optical properties primarily due to particulate backscattering.

A series of density plots of the residual waveform data from Pass 4 (flown from east to west) is shown in grey scale in Fig. 4 as well as in a color coded representation on the front cover of this issue. The color coded image shown on the front cover more clearly illustrates the features under consideration and should be referred to during this and subsequent discussions of the residual waveform density plots. The density plot of a representative portion of the residual waveform data obtained in the Sargasso Sea on Pass 4 is labeled as segment *a* in the figure. The geographical locations of this and the other similarly labeled backscatter density plots are given in Fig. 2. The horizontal axis in the plot represents elapsed flight time or along-track distance (with each major tick mark representing ~6 km), while the vertical axis spans ~30 m of depth. Although the Tektronix R-7912 temporal waveform digitizer was set to provide ~50 m of depth measurement, the system resolution during the experiment restricted the usable measurement range to ~30 m in the environmental conditions found on the shelf. The comparatively small pulse-to-pulse variability is an indication of the effectiveness of the environmental subtraction technique for removing the amplitude related system response from the residual waveforms.

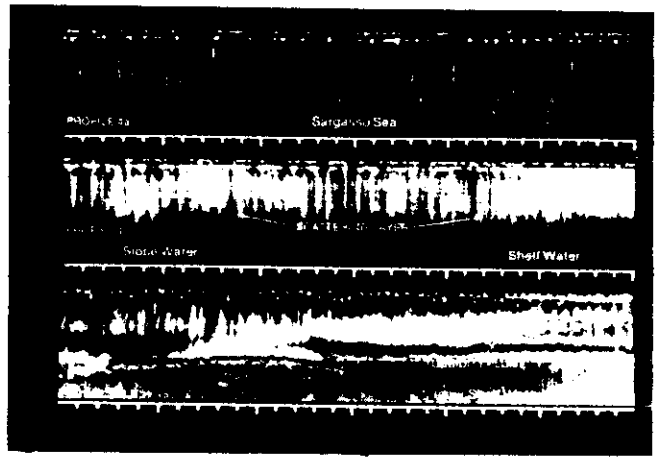

Fig. 4. Density plot of the backscatter profiles as developed from temporal waveforms to which environmental subtraction has been applied: (a) Sargasso Sea region; (b) slope water region; (c) inner shelf-water region. The geographical location of each of these regions is identified as 4*a*, 4*b*, 4*c*, respectively, in Fig. 2.

The low residual backscatter seen on the plot would, of course, be expected since the clear water matrix was developed from the Sargasso Sea observations of which this data set is a part. However, the actual base level of particulate backscatter contained in the Sargasso Sea observations will become apparent in a relative sense as the clear water waveforms are differenced from data acquired over the other water masses to form positive residuals.

A density plot of the residual waveform data from pass 4 beginning in the vicinity of the shelf break (eastern portion of the pass) and extending across the slope and shelf water masses (to point *B* in Fig. 2) is shown as *b* (Fig. 4 and front cover). In this figure, only every twenty-fourth laser measurement has been plotted to permit the bulk of the shelf and slope water masses to be viewed in a single illustration. Note the distinct patterns of subsurface backscatter that are apparent in the vicinity of the shelf break (near the beginning of the pass) and along the inner shelf (near the end of the pass).

A density plot of residual waveforms obtained for the inner section of pass 4 is presented as *c* (Fig. 4 and front cover). The positions of the sea floor and the scattering layer are labeled within the figure. The backscattered temporal waveform shown in Fig. 3 was extracted from the data at the point in the figure labeled *W*. The patchy backscatter which was apparent over much of the inner shelf is obvious near the beginning of the plot. The strong crescent-shaped bottom return from the shoal is a prominent feature in this section. A distinct plume is apparent from the strong backscatter commencing near the top of the shoal. From the pattern shown in the backscattered laser return, the plume initially appears along the eastern edge of the shoal. As the aircraft proceeded from east to west, the plume appears higher in the water column and can be seen to widen. The area of strongest backscatter appears ~7 km west of the shoal.

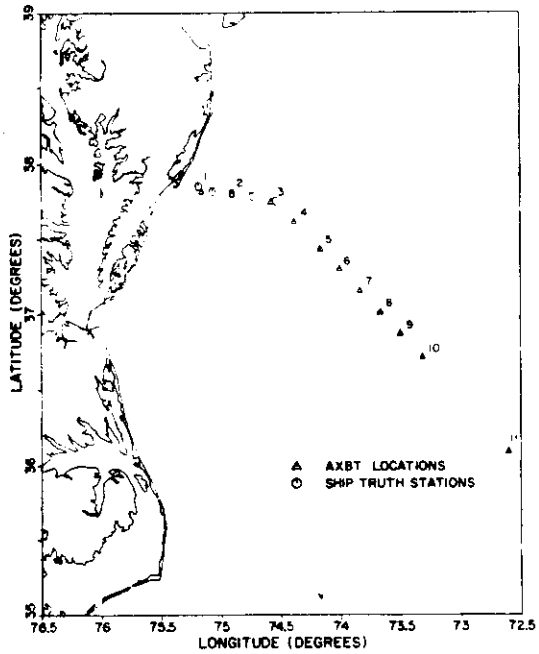

Fig. 5. Geographic locations of the ship truth stations and the airborne expendable bathythermograph drops conducted during the scattering layer mission.

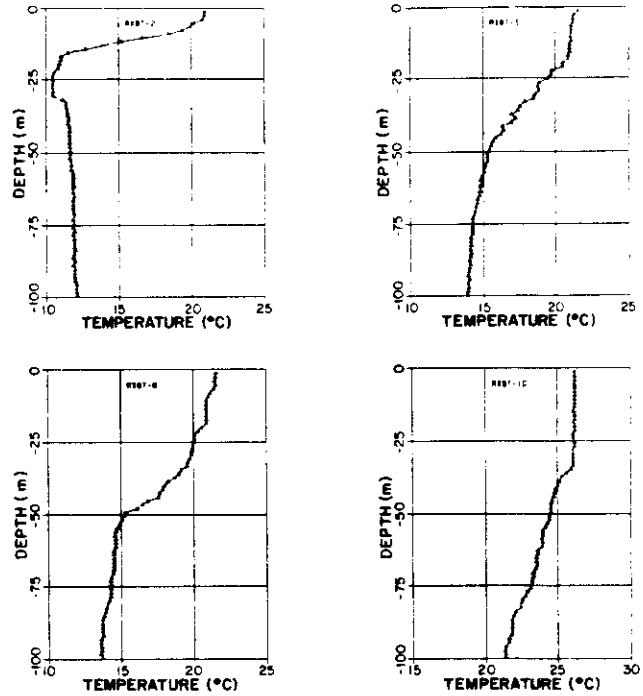

Fig. 6. Typical temperature profiles obtained from AXBT drops during the scattering layer mission. AXBT-2 shows a distinct well-developed thermocline in the inner shelf region where the scattering layer plume was seen [see Fig. 4(c)].

Thereafter, the plume begins to break down and to lose gradually its distinct identity, finally appearing as a series of patches.

During the investigation twelve AXBTs were deployed over the study area to ascertain the approximate temperature structure of the water column for aid in interpreting the airborne scattering layer information. The locations of these observations are given in Fig. 5. Temperature profiles at stations 2, 5, 8, and 10 are plotted as a function depth in Figs. 6. The temperature profiles indicate that a relatively shallow thermocline had developed at the time of the experiment beginning at a depth of 6–8 m at the inner stations and at progressively deeper depths further east on the shelf.

The locations of the five ship truthing stations are also shown in Fig. 5. The temperature and beam attenuation coefficient alpha (obtained from the beam transmissometer readings) data obtained from the truthing vessel are plotted as a function of depth in Fig. 7. No beam transmissometer data were available for station 5 due to an electronic problem. The temperature profiles obtained from the chartered vessel are in reasonable agreement with the temperature profiles from the AXBTs. The profile of alpha at the innermost station reveals a rather pronounced layer of turbidity several meters above the bottom. The profile at station 2 indicates almost no change in transmission with depth. Relatively small inflections in the transmissivity profiles at Stations 3 and 4 are indicated at depths of 16 and 23 m, respectively.

The general objective of the field investigation was to determine the performance characteristics of AOL electrooptical components and to establish the poten-

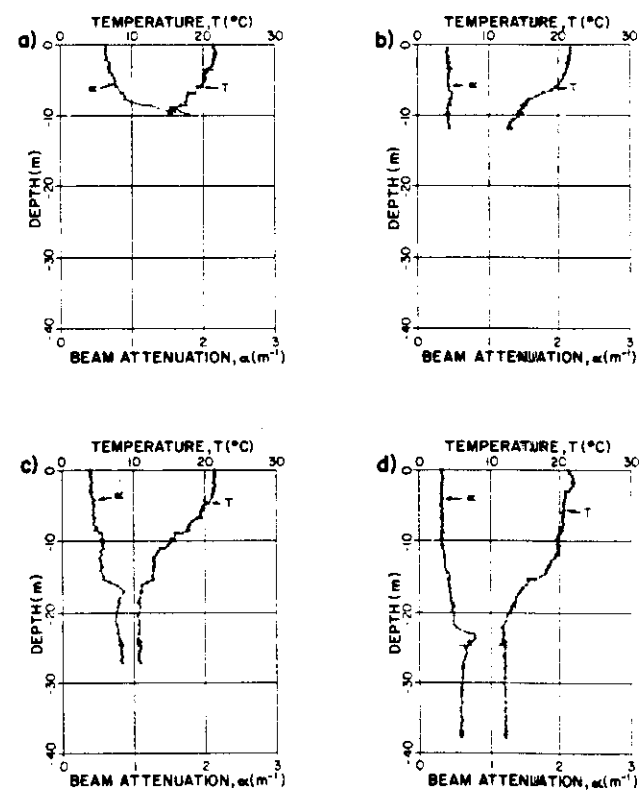

Fig. 7. Typical beam attenuation and temperature profiles obtained by the surface truth vessel. The sequential geographic locations of these data are given in Fig. 5.

tial feasibility for measuring scattering layers with an airborne laser system. These objectives could be addressed without surface truthing support. Accordingly, only a relatively modest support effort was mounted during the brief period just prior to the flight. No provision was made to determine the types of particulate matter responsible for the observed scattering layers. Finally, since it was not realized that a significant scattering layer or plume would be detected inside the shoal area, no station was taken landward of the shoals. In spite of the limitations and lack of simultaneity of the surface truthing stations with the bulk of the airborne observations, the surface truthing is still of considerable value in interpreting the airborne results.

During the flight, elevated backscatter from within the water column was observed in the vicinity of shoals flanking the coast of Assateague Island over the inner shelf and in slope waters near the Gulf Stream. Although the particulate matter responsible for the scatter in these different water masses was not specifically identified, we suggest that the scattering layers observed in the slope water near the Gulf Stream and on the outer shelf were due to elevated phytoplankton concentrations. By contrast, the plume observed to originate near the shoal was likely due to the entrainment of suspended sediments into the water column. Measurements of winds prior to and during the experiment as well as the surface truthing observations at Station 1 support this latter hypothesis.

Observations of wind speed and direction made at Wallops Flight Facility (located ~13 km inland from the coast) distinctly indicated the presence of an east wind during the period prior to the experiment and a south wind during the experiment. In-flight wind observations made during the experiment (from an altitude of 300 m with the aircraft inertial navigation system) indicated a wind velocity of ~20 knots from the southeast. Measurements obtained with the beam transmissometer at stations located immediately seaward of the shoaled area indicated the presence of a fairly dense layer of fluff covering the sea floor. The presence of this layer of flocculated particulate matter near the inner portion of the shelf is fairly common, especially during the late spring and summer months when wind events of sufficient strength to redistribute the material within the water column are infrequent. Although the westerly flow of water coupled with surface wave action may have been reworking fine material from the shoal, it is more likely that the wind driven westerly flow of water had coupled to sufficient depth to push the relative shallow bottom water over the shoal extruding the layer of fluff into the water column. A similar trend, although less apparent, was observed on Pass 3 flown over the shoal from west to east. It is not expected that any significant portion of the scattering was related to ocean bubbles. Bubble concentrations decrease exponentially with depth and typically have $1/e$ depths of only ~1.5 m.[34]

V. Summary and Conclusions

A submerged oceanic plume in the near coastal/shelf waters of the northwestern Atlantic Ocean has been detected and mapped in the vertical plane using airborne lidar on-wavelength depth-resolved backscatter methods. Backscattered laser light from particulate matter was also acquired during the transect over the outer shelf and slope water masses. Strong undesired reflections from the air–water interface were successfully managed by the use of nonoptimal spatial filtering, off-nadir operation, and adjustment of the waveform digitizer gain. The presence of thermal stratification of the water column was verified by the use of AXBTs and sea truthing, which also provided measurements of transmission of the water column. Although the sources of particulate matter responsible for producing the laser backscatter were not specifically identified, it is felt that elevated phytoplankton concentrations were responsible for the scatter observed in the slope and outer shelf water masses. The presence of the turbid bottom water east of the shoal (coupled with the sustained east wind before and during the flight experiment) suggests that the resuspension of the bottom sediments over the shoal (and a wind driven westerly drift of the water column) were responsible for the observed plume.

New and more optimal filtering in the telescope focal plane is currently being implemented. This modification is expected to significantly reduce the Fresnel backscatter from the air–water interface. In addition a gated photomultiplier tube with appropriate gain control is being configured to compensate for the exponential attenuation of signal with depth in the water column. It is expected that the gated photomultiplier tube will be able to compensate for the loss over six or seven attenuation lengths. These techniques are to be tested in future field investigations to determine their effectiveness and to ascertain the degree to which the technique can be utilized during daylight hours. Daylight operation would allow the simultaneous acquisition of passive ocean color data and the conduct of important correlative active–passive studies.

The authors wish to extend their personal thanks to the persons involved with the scientific field experiment, the AOL project, and aircraft operations. We are particularly indebted to the Department of Energy for the loan of the frequency-doubled Nd:YAG laser used to obtain the scattering layer data. We also thank the Ocean Processes Branch of NASA Headquarters for continued support and encouragement.

References

1. Committee on Earth Sciences, "A Strategy for Earth Science from Space in the 1980's and 1990's," in *Part II: Atmosphere and Interactions with the Solid Earth, Oceans, and Biota*, National Research Council (National Academy Press, Washington, DC, 1985), pp. xiii and 89.

2. R. W. Eppley, E. Stewart, M. R. Abbott, and U. Herman, "Estimating Ocean Primary Production from Satellite Chlorophyll: Introduction to Regional Differences and Statistics for the Southern California Bight," J. Plankton Res. **7,** 57 (1985).
3. P. G. Falkowski, Ed., *Primary Productivity in the Sea* (Plenum, New York, 1980), p. v.
4. T. Platt and A. W. Herman, "Remote Sensing of Phytoplankton in the Sea: Surface-Layer Chlorophyll as an Estimate of Water-Column Chlorophyll and Primary Production," Int. J. Remote Sensing **4,** 343 (1983).
5. W. G. Harrison, T. Platt, R. Calienes, and N. Ochoa, "Photosynthetic Parameters and Primary Production of Phytoplankton Populations off the Northern Coast of Peru," in *Coastal Upwelling*, F. A. Richards, Ed. (American Geophysical Union, Washington, DC, 1981), pp. 303–311.
6. L. R. Poole and W. E. Esaias, "Water Raman Normalization of Airborne Laser Fluorosensor Measurements: A Computer Model Study," Appl. Opt. **21,** 3756 (1982).
7. R. C. Smith and K. S. Baker, "The Bio-Optical State of Ocean Waters and Remote Sensing," Limnol. Oceanogr. **23,** 247 (1978).
8. F. E. Hoge, R. N. Swift, and E. B. Frederick, "Water Depth Measurement Using an Airbone Pulsed Neon Laser System," Appl. Opt. **19,** 871 (1980).
9. R. A. O'Neil, "Coastal Hydrography Using the CCRS Lidar Bathymeter," in *The Conference on Ocean Environment and Its Interactions with Offshore Structures*, Goteborg '83, 1–4 Mar. 1983 (The Swedish Trade Fair Foundation, 1983), p. 10.
10. O. Steinvall, H. Klevebrant, J. Lexander, and A. Widen, "Laser Depth Sounding in the Baltic Sea," Appl. Opt. **20,** 3484 (1981).
11. B. Billard, T. H. Abbot, and M. F. Penny, "Airborne Estimation of Sea Turbidity Parameters from the WRELADS Laser Airborne Depth Sounder," Appl. Opt. **25,** 2080 (1986).
12. K. Muirhead and A. P. Cracknell, "Airborne Lidar Bathymetry," Int. J. Remote Sensing **7,** 497 (1986).
13. F. E. Hoge and R. N. Swift, "Active–Passive Correlation Spectroscopy: A New Technique for Identifying Ocean Color Algorithm Spectral Regions," Appl. Opt. **25,** 2571 (1986).
14. J. R. Proni, F. C. Newman, F. Ostapoff, and D. J. Walter, "Vertical Particulate Spires or Walls within the Florida Current and near the Antilles Current," Nature, London **276,** 360 (1978).
15. J. R. Apel, H. M. Byrne, H. R. Proni, and R. L. Sellers, "A Study of Oceanic Internal Waves Using Satellite Imagery and Ship Data," Remote Sensing Environ. **5,** 125 (1976).
16. J. R. Apel, J. R. Proni, H. M. Burne, and R. L. Sellers, "Near-Simultaneous Observations of Intermittent Internal Waves of the Continental Shelf from Ship and Spacecraft," Geophys. Res. Lett. **2,** 128 (1975).
17. S. C. Lubard, L. R. Thebaud, and R. F. Lutomirski, "Lidar Remote Sensing of Internal Waves and Optical Properties," in Advisory Group for Aerospace Research and Development (*AGARD*) Symposium on "Propagation Factors Affecting Remote Sensing by Radio Waves," held in Oberammergau, Federal Republic of Germany, May 24–28, 1983, sponsored by the Electromagnetic Wave Propagation Panel of AGARD, pp. 39-1–39-13.
18. D. M. Phillips, "The Effect of Water Turbidity of Laser Depth Sounding Performance," in *Proceedings, Fourth Laser Hydrography Symposium*, 30 Sept.–3 Oct. 1980, Document AR-002-576, Report ERL-193-SD, M. F. Penny and D. M. Phillips, Eds., Adelaide, Australia, Mar. 1981.
19. F. E. Hoge and R. N. Swift, "Airborne Detection of Oceanic Turbidity Cell Structure Using Depth-Resolved Laser-Induced Water Raman Backscatter," Appl. Opt. **23,** 3778 (1983).
20. F. E. Hoge and R. N. Swift, "Application of the NASA Airborne Oceanographic Lidar to the Mapping of Chlorophyll and Other Organic Pigments," in *Chesapeake Bay Plume Study Superflex 1980*, NASA Conf. Publ. 2188 (U.S. GPO, Washington, DC, 1981), pp. 349–374.
21. F. E. Hoge and R. N. Swift, "Airborne Simultaneous Spectroscopic Detection of Laser-Induced Water Raman Backscatter and Fluorescence from Chlorophyll *a* and Other Naturally Occurring Pigments," Appl. Opt. **20,** 3197 (1981).
22. F. E. Hoge and R. N. Swift, "Airborne Dual Laser Excitation and Mapping of Phytoplankton Photopigments in a Gulf Stream Warm Core Ring," Appl. Opt. **22,** 2272 (1983).
23. F. E. Hoge and R. N. Swift, "Airborne Mapping of Laser-Induced Fluorescence of Chlorophyll *a* and Phycoerythrin in a Gulf Stream Warm Core Ring," Paper 18 in *Mapping Strategies in Chemical Oceanography*, A. Zirino, Ed. (American Chemical Society, Washington, DC, 1985), pp. 353–372.
24. F. E. Hoge and R. N. Swift, "Experimental Feasibility of the Airborne Measurement of Absolute Oil Fluorescence Spectral Conversion Efficiency," Appl. Opt. **22,** 37 (1983).
25. F. E. Hoge and R. N. Swift, "Oil Film Thickness Measurement Using Airborne Laser-Induced Water Raman Backscatter," Appl. Opt. **19,** 3269 (1980).
26. F. E. Hoge and R. N. Swift, "Absolute Tracer Dye Concentration Using Airborne Laser-Induced Water Raman Backscatter," Appl. Opt. **20,** 1191 (1981).
27. F. E. Hoge, W. B. Krabill, and R. N. Swift, "The Reflection of UV Laser Pulses from the Ocean," Mar. Geod. **8,** 313 (1984).
28. J. L. Bufton, F. E. Hoge, and R. N. Swift, "Airborne Measurements of Laser Backscatter from the Ocean Surface," Appl. Opt. **22,** 2603 (1983).
29. W. B. Krabill, J. G. Collins, L. E. Link, R. N. Swift, and M. L. Butler, "Airborne Laser Topographic Mapping Results," Photogramm. Eng. Remote Sensing **50,** 685 (1984).
30. R. Nelson, W. B. Krabill, and G. Maclean, "Determining Forest Canopy Characteristics Using Airborne Laser Data," Remote Sensing Environ. **15,** 201 (1984).
31. F. E. Hoge, R. N. Swift, and J. K. Yungel, "Feasibility of Airborne Detection of Laser-Induced Fluorescence Emissions from Green Terrestrial Plants," Appl. Opt. **22,** 2991 (1983).
32. F. E. Hoge, R. E. Berry, and R. N. Swift, "Active–Passive Airborne Ocean Color Measurement: 1. Instrumentation," Appl. Opt. **25,** 39 (1986).
33. F. E. Hoge, R. N. Swift, and J. K. Yungel, "Active–Passive Airborne Ocean Color Measurement: 2. Applications," Appl. Opt. **25,** 48 (1986).
34. G. B. Crawford and D. M. Farmer, "On the Spatial Distribution of Ocean Bubbles," J. Geophys. Res. **92,** 8231 (1987).